Journal of Energy Chemistry 27 (2018) 395–403

Contents lists available at ScienceDirect

Journal of Energy Chemistry

journal homepage: www.elsevier.com/locate/jechem

http://www.journals.elsevier.com/journal-of-energy-chemistry/

Active sites contribution from nanostructured interface of palladium and cerium oxide with enhanced catalytic performance for alcohols oxidation in alkaline solution

Fulong Wang[a], Huaguang Yu[a], Zhiqun Tian[b], Huaiguo Xue[a], Ligang Feng[a,*]

[a] School of Chemistry and Chemical Engineering, Yangzhou University, Yangzhou 225002, Jiangsu, China
[b] Collaborative Innovation Center of Renewable Energy Materials, Guangxi University, Nanning 530004, Guangxi, China

ARTICLE INFO

Article history:
Received 27 November 2017
Revised 14 December 2017
Accepted 15 December 2017
Available online 20 December 2017

Keywords:
Alcohols oxidation
Fuel cells
Pd catalysts
Electrooxidation
CO stripping

ABSTRACT

Nanostructured interface is significant for the electrocatalysis process. Here we comparatively studied the electrooxidation of alcohols catalyzed by nanostructured palladium or palladium–cerium oxide. Two kinds of active sites were observed in palladium–cerium oxide system, attributing to the co-action of Pd–cerium oxide interface and Pd sites alone, by CO stripping technique, a structure-sensitive process generally employed to probe the active sites. Active sites resulting from the nanostructured interfacial contact of Pd and cerium oxide were confirmed by high resolution transmission electron microscopy and electrochemical CO stripping approaches. Electrochemical measurements of cyclic voltammetry and chronometry results demonstrated that Pd–cerium oxide catalysts exhibited much higher catalytic performances for alcohols oxidation than Pd alone in terms of activity, stability and anti-poisoning ability. The improved performance was probably attributed to the nanostructured active interface in which the catalytic ability from each component can be maximized through the synergistic action of bi-functional mechanism and electronic effect. The calculated catalytic efficiency of such active sites was many times higher than that of the Pd active sites alone. The present work showed the significance of valid nanostructured interface design and fabrication in the advanced catalysis system.

1. Introduction

Nanostructured Pd-based catalysts are significant to the electrooxidation of alcohols, an important half reaction in direct alcohols fuel cells that are considered to satisfy the increasing demands of high power density at low cost for technological developments [1–6]. It has long been accepted that exploring highly efficient catalysts for alcohols oxidation is urgent for the current fuel cells technology development due to the usage of noble metals [7,8]. With this goal in mind, quite a lot of works have been done to reduce the noble metal loading and increase the activity and durability by exploring novel hybrid catalyst materials [9–13].

A bi-functional mechanism of alcohols electrooxidation based on a Pt–Ru material is well recognized, in which the Pt provides active sites for the adsorption and oxidation of alcohols molecular and the neighboring Ru offers the oxygen-containing species for the oxidation of intermediates produced during the alcohols oxidation [10,14,15]. The electronic effect in atomic scale from the interaction of different components in the catalyst system is significant in understanding the performance improvements [16]. Deriving from the above mechanisms, noble metals like Pt and Pd in combination with the transition metal oxides were intensively developed and significant advances were made to push the development of fuel cells catalyst industries [17–20]. For example, platinum–nickel hydroxide was reported to have excellent catalysis activity and durability for methanol oxidation in alkaline solution, due to the combined contribution from each component and the electronic effect via interaction of individuals [21]; La_2O_3 can promote formic acid oxidation over Pd catalyst because of the improved electron transfer during electrochemical reaction [22]; other kind of metal oxides like Co_3O_4 [23], MnO_2 [24] and TiO_2 [25] have been demonstrated to exhibit improved catalytic activity and durability for alcohols oxidation.

It is happy to see many advanced catalyst materials proposed in recent years, however if we take a look at the work carefully, there are still some flaws or imperfection in understanding the origin of performance [26]. For the catalysts system proposed, the heterostructure of the active sites and neighboring promotion sites

* Corresponding author.
E-mail address: ligang.feng@yzu.edu.cn (L. Feng).

https://doi.org/10.1016/j.jechem.2017.12.011

surely can guarantee the catalysis process of adsorption and charge transfer, and the promotion effect in all work was attributed to the synergistic effect of the catalyst components in the system. Unfortunately, by surveying the literatures, we do not find directly evidence from the electrochemical measurements, though the connection interface was claimed visible in the microscopic images [27]. Moreover, it is still not clear how the interface active sites contributed to the improved activity. It is highly desirable that if we could observe some clues from the electrochemical measurements to confirm these active sites from the nano-interface contact and analyze the contribution to the improved performance.

Pd–cerium oxide system was reported as a highly efficient catalyst for alcohols oxidation according to the bi-functional mechanism and electronic effect [28]. Because cerium oxide has multi-valences that can provide enough oxygen-containing species during the electrochemical oxidation process, it was thought as an efficient assistant-catalyst in alcohols oxidation. Though the effect of fabrication approaches was intensively studied and the promotion effect of oxide was evident, probing the promotion effect in depth is still going on due to the complicated effect in this catalyst system that involves the metal oxide state, surface compositions, electronic effect and so on [29,30]. Herein, back to our concerns, there is no active sites evaluation in the catalyst characterization or even no relevant reports to disclose the active sites contribution to catalytic performance. In the current study, we re-scrutinized the Pd–cerium oxide system for alcohols oxidation in the alkaline solutions to probe the possible active sites contribution to the catalytic performance improvement. In considering the multiple valence states of cerium oxide, it was shortened as CeO_x in the present work. A common approach for Pd based catalyst preparation was employed in which Pd nanoparticles were anchored on the surface of hybrid support; with this method, different active sites were anticipated to form by anchoring Pd particles on the carbon surface or CeO_x surface. The catalyst material was thoroughly measured and characterized; as expected, we find the consistence not only from the physical characterizations but also from the electrochemical CO stripping measurements. We also for the first time analyzed the activity contributions from the different active sites presented in the system and found the active sites from nanostructured interface are more active and efficient in the electro-catalysis process. The importance of forming nano-interface from multiple components is emphasized for the highly active electrode materials preparation. The results are significant in understanding the catalysis mechanism and developing new hybrid nano-catalysts material.

2. Experimental

2.1. Preparation of Pd–CeO_x/C

The CeO_x/C support was prepared as follows: A given amount of Ce_2O_3 was dissolved in 15 mL of concentrated HNO_3 and then diluted in 100 mL mixed solution of ultrapure water and ethanol (1:1 in volume ration). Then, a given amount of Vulcan XC-72 carbon was ultrasonically dispersed into the above solution, and the solution was kept at room temperature (25 °C) under vigorous agitation for 4 h. After stirring, 1 M NaOH and 0.5 M Na_2CO_3 solution were added in turn into the mixture to form precipitates. Subsequently, the suspension was stirred overnight and finally filtered and the solid was transferred to a tubular oven at 550 °C for 3 h under the protection of N_2 to obtain a stable CeO_x/C support.

In the second step, the Pd–CeO_x/C catalyst was synthesized. First, a given amount of CeO_x/C hybrid support and H_2PdCl_4 solution were ultrasonically dispersed in 50 mL of ethylene glycol. And then the pH of the suspension was adjusted to about 11 by adding 1 M NaOH solution dropwise slowly under sonication. After that, the suspension was kept at room condition for 1 h. The resulting suspension was placed in the middle of a microwave oven operating at 700 W for 60 s on and 15 s off in turn for three times and cooled to room temperature naturally. Finally, the suspension was filtered, washed and dried overnight at 70 °C in a vacuum oven. All solutions were prepared using Thermo Fisher Scientific (USA) Co. Ltd. ultrapure water and analytical-grade reagents. For a valid comparison, home-made Pd/C catalyst 20 wt% was also prepared by the same approach. All of the materials were purchased and used without further purification.

2.2. Physical characterizations

Transmission electron microscopy (TEM) and element mapping analysis were conducted on a TECNAI G2 operating at 200 kV. Samples were sonicated and dispersed in ethanol and placed dropwise onto a copper support grid for TEM observation.

Scanning electron microscopy (SEM) and energy dispersive X-ray detector spectrum (EDS) measurements were performed with an XL30 ESEM FEG field emission scanning electron microscope to determine the morphology.

X-ray photoelectron spectroscopy (XPS) measurements were carried out on an ESCALAB250Xi spectrometer with an Al $K\alpha$ radiation source.

X-ray diffraction (XRD) measurements were performed with a PW1700 diffractometer (Philips Co.) using a Cu $K\alpha$ ($\lambda = 1.5405$ Å) radiation source operating at 40 kV and 40 mA. A fine powder sample was grinded, then put into the glass slide and pressed to make a flat surface under the glass slide.

2.3. Electrochemical measurements

All the electrochemical measurements were carried out on an INTERFACE 1000 potentiostat/galvanostat (GAMRY INSTRUMENTS Co., USA) and a conventional three-electrode test cell was employed. The saturated calomel electrode (SCE, Hg Hg_2Cl_2) was used as reference electrode. All of the potentials were relative to the SCE electrode. A Pt plate with 10 cm^{-2} was used as a counter electrode. A glassy carbon electrode coated by thin film catalyst (diameter $d = 3$ mm) was used as a working electrode.

Cyclic voltammetry measurements were carried out in 1 M KOH electrolyte and purged with high-purity N_2 to remove dissolved oxygen. Electrochemical experiments of methanol oxidation were performed in 1 M KOH containing 1 M methanol solution and ethanol oxidation was performed in 1 M KOH containing 1 M ethanol solution. All solution preparations were supplied by ultrapure water. All glass electrodes were cleaned by polishing with 0.05 μm alumina powder suspension (water) followed by ultrasonic cleaning in deionized water before use.

2.4. Electrochemical pre-treatment

The catalyst ink was prepared by ultrasonically dispersing a mixture containing 5 mg of catalyst, 950 μL of ethanol and 50 μL of a 5 wt% Nafion solution. Next, 5 μL of the catalyst ink was pipetted onto a pre-cleaned working electrode.

2.5. CO stripping

The adsorbed carbon monoxide (CO_{ad}) stripping voltammetry was measured in a 1 M KOH solution. CO was purged into the KOH solution for 15 min to allow the complete adsorption of CO onto the catalyst when the working electrode was kept at −0.8 V (vs. SCE), and excess CO in the electrolyte was purged out with N_2 for 15 min. The amount of CO_{ad} was evaluated by integration of the CO_{ad} stripping peak, assuming 420 μC cm^{-2} of coulombic charge required for the oxidation of the CO monolayer.

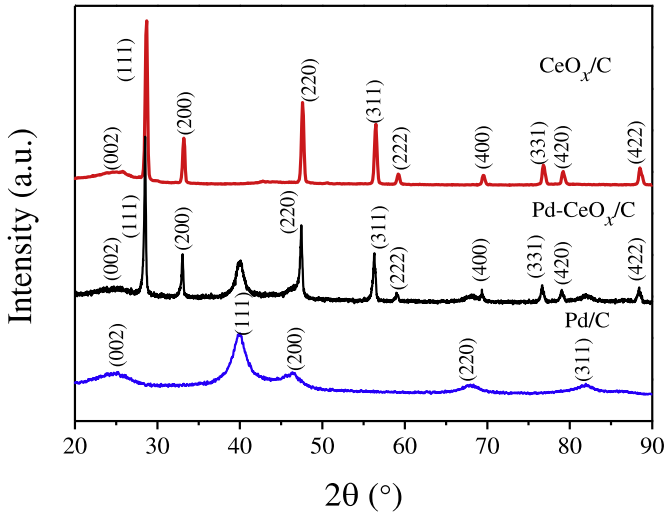

Fig. 1. XRD patterns of Pd–CeO_x/C catalyst, CeO_x/C support and Pd/C catalyst.

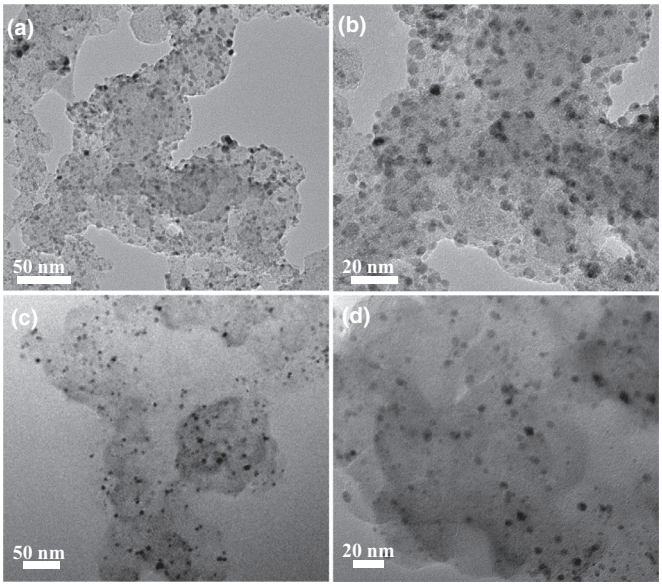

Fig. 2. TEM images of Pd–CeO_x/C catalyst (a, b) and Pd/C catalyst (c, d). Scale bars for (a) and (c): 50 nm; (b) and (d): 20 nm.

2.6. Cyclic voltammetry measurements

The activity of metal nanoparticles for methanol and ethanol electro-oxidation was measured. The measurements were carried out at room temperature in 1 M KOH containing 1 M methanol solution or 1 M KOH containing 1 M ethanol solution at potential range between −1.0 and 0.2 V (vs. SCE).

2.7. Electrochemical impedance measurements

The electrochemical impedance spectra (EIS) were recorded at the frequency range from 1000 kHz to 10 mHz with 15 points per decade. The amplitude of the sinusoidal potential signal was 5 mV.

3. Results and discussion

The crystal structure of hybrid Pd–CeO_x/C was characterized by X-ray diffraction (XRD) measurements, and the characteristic pattern was shown in Fig. 1. It is noted that the characteristic peaks of face-centered-cubic (FCC) structure of cerium oxide were obviously observed in the CeO_x/C support indicating the successfully fabrication of aimed materials. These peaks were well kept after Pd nanoparticles were deposited on CeO_x/C surface; meanwhile, the characteristic peaks of FCC phase of Pd at 40, 46, 68 and 82 degrees were clearly observed in consistent with those peaks observed in Pd/C catalyst. From the XRD pattern of Pd–CeO_x/C sample, the mixed crystal structure was formed as expected. The crystal size calculated by the Scherrer formula based on (2 2 0) peak was around 3.5 nm and 3.63 nm for the Pd–CeO_x/C and Pd/C catalyst respectively. The morphology of the prepared Pd–CeO_x/C and Pd/C samples was probed by transmission electron microscopy (TEM) and the images were shown in Fig. 2. The Pd nanoparticles were uniformly distributed over the support in both Pd–CeO_x/C and Pd/C samples; the average particle size by counting randomly 150 particles was 3.61 nm and 3.86 nm for Pd–CeO_x/C and Pd/C separately with a narrow size distribution (Fig. S1).

The high resolution transmission electron microscopy (HRTEM) was employed to examine the nanostructured interface formed in the catalyst system, and some typical images were shown in Fig. 3. One can clearly see the fringe lattice as addressed for the corresponding nanoparticles; the hybrid unit consisted of Pd and cerium oxide and carbon support were observed that might be beneficial to the catalysis process as the neighboring connection of Pd, CeO_x and carbon can provide the necessary boundaries for adsorption, charge transfer and conductivity etc. (Fig. 3(a) and (b)). Similar case was also found in the catalyst system of Pd–Ni_2P, Pd–CoP [19,31]. The element mapping was done on a randomly selected area, the elements of Pd, Ce, O and carbon were uniformly visible over the support (Fig. 3(c–i)). The composition of the aimed Pd–CeO_x/C catalyst was analyzed by EDX (Fig. S2) and the weight percentage of Pd and Ce was approximately 20.62%, 14.21% respectively; for Pd/C sample, the weight percentage of Pd was approximately 19.45%, which was also close to the nominal contents (Fig. S3).

Surface analysis of the Pd–CeO_x/C was carried out using X-ray photoelectron spectroscopy (XPS), the C 1*s* value of 284.6 eV was used as references to calibrate all the peaks. The Pd 3*d* spectra of the Pd–CeO_x/C and Pd/C catalysts were compared in Fig. 4(a). For the Pd/C catalyst, the peaks at 335.26 eV and 340.45 eV are attributed to metallic Pd (0), and Pd (II) species located at respectively 336.30 eV and 341.55 eV. Analogously, for the Pd–CeO_x/C catalyst, the peaks at 335.71 eV and 340.93 eV are attributed to metallic Pd, whereas the peaks at 336.90 eV and 342.47 eV are assigned to Pd (II) species respectively. By comparing the peaks position, an evident shift of ca. 0.5 eV was observed to the high binding energy (BE) direction for Pd 3*d* in the Pd–CeO_x/C catalyst which indicated an electronic interaction between the CeO_x support and Pd nanoparticles [32]. Similar results were reported on the Pt–CeO_x materials, in which the partial electron transfer from Pt surface to cerium oxide was thought due to the redox reaction between Pt and high oxidation state of cerium, and the details chemical equations can be found in the cited reference here [32]. This electronic effect can modify the electronic and catalytic properties of metal nanoparticles and the matrix by activating the surface state toward electrode processes, which is important for the electrochemical reactions.

Fig. 4(b) presented the results of analyzing Ce 3*d* XPS spectrum recorded from the Pd–CeO_x/C sample. The whole peak could be deconvoluted to Ce $3d_{3/2}$ and $3d_{5/2}$ peaks, the energy separation between the two spin–orbit levels was found to be 18.4 ± 0.2 eV, that was consistent with previous data [33]. The binding energy peaks at 882.9 eV, 889.3 eV, 898.8 eV, 901.2 eV, 907.5 eV, 917.2 eV are related to Ce^{4+} species while the peaks at BEs of 881.3 eV, 885.3 eV, 899.5 eV, 903.9 eV are assigned to Ce^{3+} species [34]. All deconvolution peaks were used to calculate the relative contributions

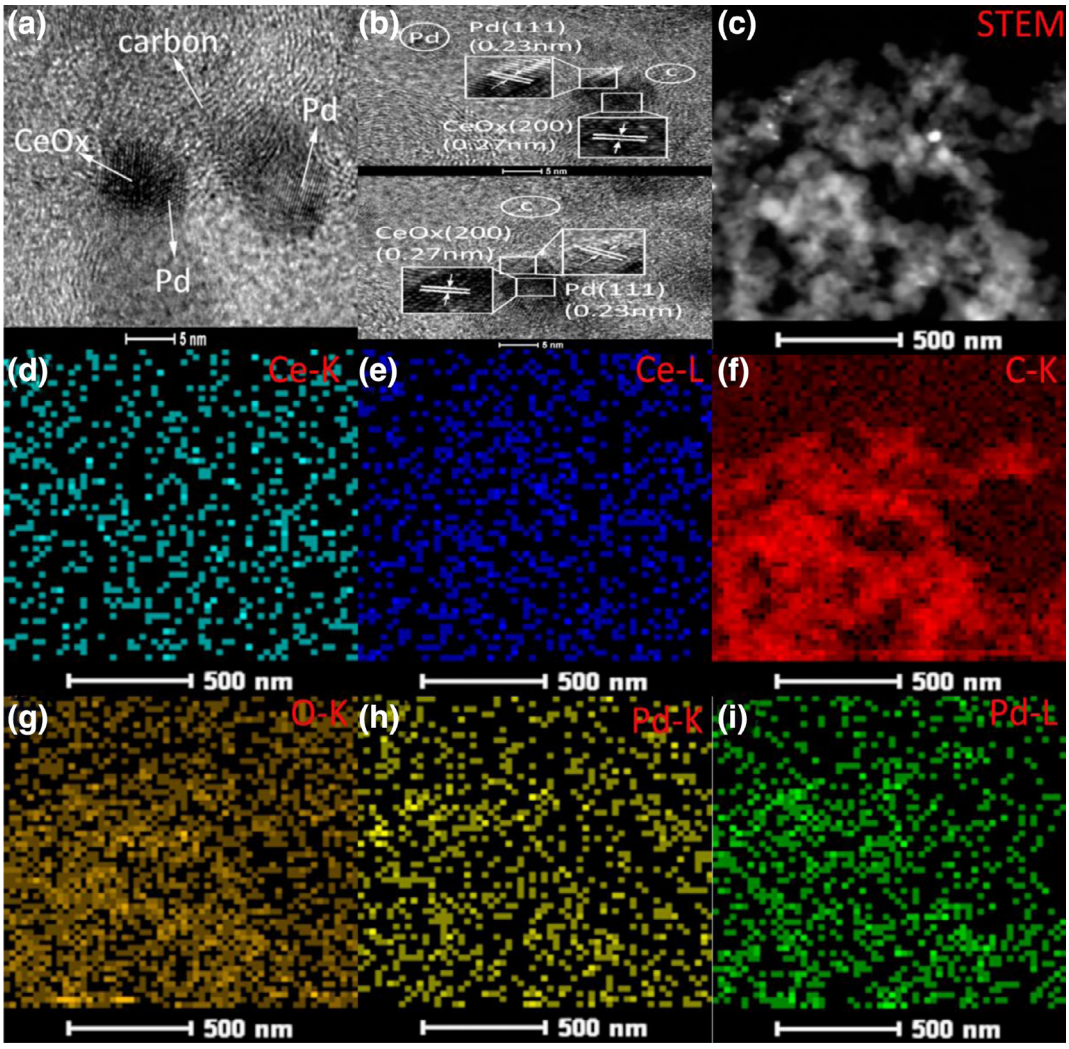

Fig. 3. (a, b) HR-TEM (scale bar: 5 nm) images of Pd–CeO_x/C sample; (c) STEM; (d–i) elemental mapping images of the Pd–CeO_x/C (scale bar: 500 nm).

of the Ce^{4+} and Ce^{3+} states on the surface [33] and it was 82% and 18%, respectively. Fig. 4(c) shows the O 1*s* XPS spectrum of Pd–CeO_x/C catalyst. It can be deconvoluted into five peaks; the main component of 530 eV peak is surely attributed to the lattice oxygen and the 531.71 eV peak to OH or adsorbed H_2O [35]; the 532.7 eV peak is associated with oxygen bound to Ce^{4+} cations in CeO_x [36], whereas the binding energy peak at 533.6 eV is associated with C–O–H or C–O–C and the peak at BE of 535.07 eV is related to O–Ce^{3+} surface bonds [37]. The abundant oxygen-containing species formed on the cerium surface was thought as a good plus to provide active sites for adsorption of intermediates and accelerate the alcohols oxidation ability.

CO electrooxidation is a structure-sensitive process that generally is employed to probe the active sites during the catalysis [38]. Here the CO stripping experiment was done to evaluate the possible active sites and the electrochemical active surface area (ECSA), and the corresponding voltammetry curves were compared in Fig. 5(a). As expected for Pd–CeO_x/C catalyst, two obvious peaks for CO oxidation were observed at −0.3 V and −0.24 V respectively indicating there were two kinds of active sites in Pd–CeO_x system. While only one peak at −0.24 V can be attributed to the CO oxidation for Pd/C catalyst and no peak was observed for the CeO_x/C support. Thus, the active sites in the Pd–CeO_x/C should come from Pd sites on carbon surface and the sites on Pd–cerium oxide interface. The perfectly match of the peak at −0.24 V in both Pd–CeO_x/C and Pd/C catalyst indicated that peak should come from the same kind of active sites, namely Pd nanoparticles. The other peak at −0.3 V, ca. 60 mV negative than the aforementioned peak, was no doubt arising from the active sites formed at the interface of Pd and cerium oxide active boundary. The peak was further fitted in order to know the contribution from two different active sites, and the peak area was employed to calculate the active sites (Fig. 5b); and it was calculated to be 58% arising from Pd active sites and the rest of 42% was from the newly formed active interface of Pd and cerium oxide. The electrochemical active surface area (ECSA) was calculated by assuming a full monolayer of CO adsorption on the Pd surface and the charge demand for oxidation is 420 μC cm^{-2}. It was calculated to be 58.3 m^2 g^{-1} and 99.9 m^2 g^{-1} for Pd/C, Pd–CeO_x/C catalysts, respectively. The electrochemical active surface area represents the available active sites for reactive molecular adsorption and oxidation; the ECSA of Pd–CeO_x/C was about 1.7 times higher than that of Pd/C catalyst, so the active sites from nano-structured interface can provide more active sites for the catalysis process though it only occupies less than half content. Specifically, if we assumed both Pd sites in Pd/C and Pd–CeO_x/C have similar activity, the electrochemical active surface area of 33.8 m^2 g^{-1} could be attributed to the Pd sites and the rest of 66.1 m^2 g^{-1} was assigned to the formed nano-interface active sites; and the efficiency of the latter was about 2.7 times higher than that of the original Pd sites.

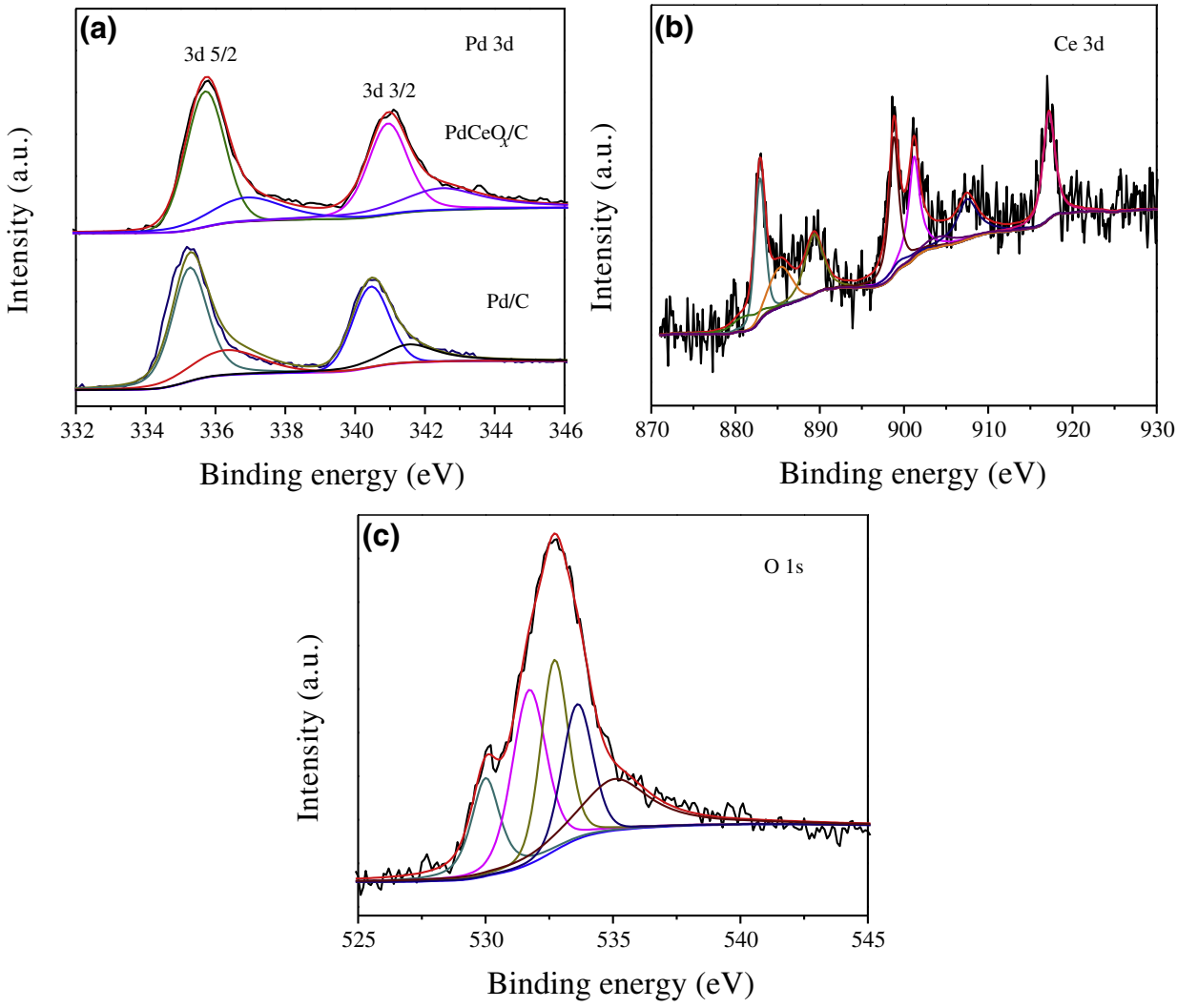

Fig. 4. XPS spectra of Pd 3*d* in Pd–CeO$_x$/C and Pd/C catalysts (a), Ce 3*d* (b) and O 1*s* (c) in Pd–CeO$_x$/C catalyst.

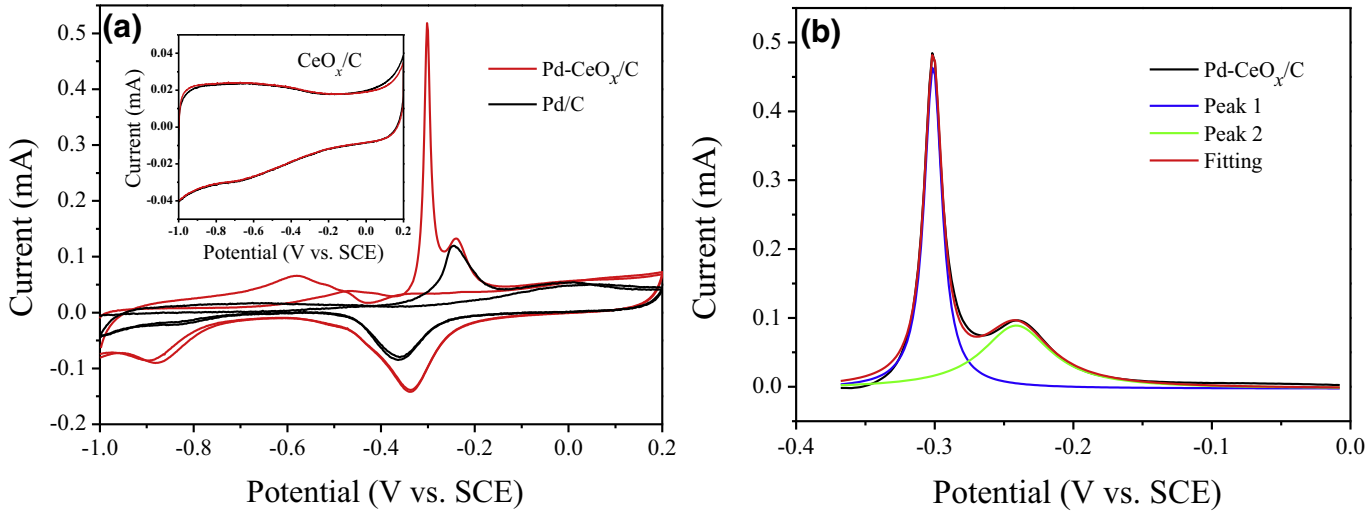

Fig. 5. CO_{ad} stripping voltammograms of Pd–CeO$_x$/C, Pd/C catalysts and CeO$_x$/C support (inset) in 1 M KOH solution at the scan rate of 20 mV s^{-1} (a) and the fitting curves of CO oxidation peaks for Pd–CeO$_x$/C (b).

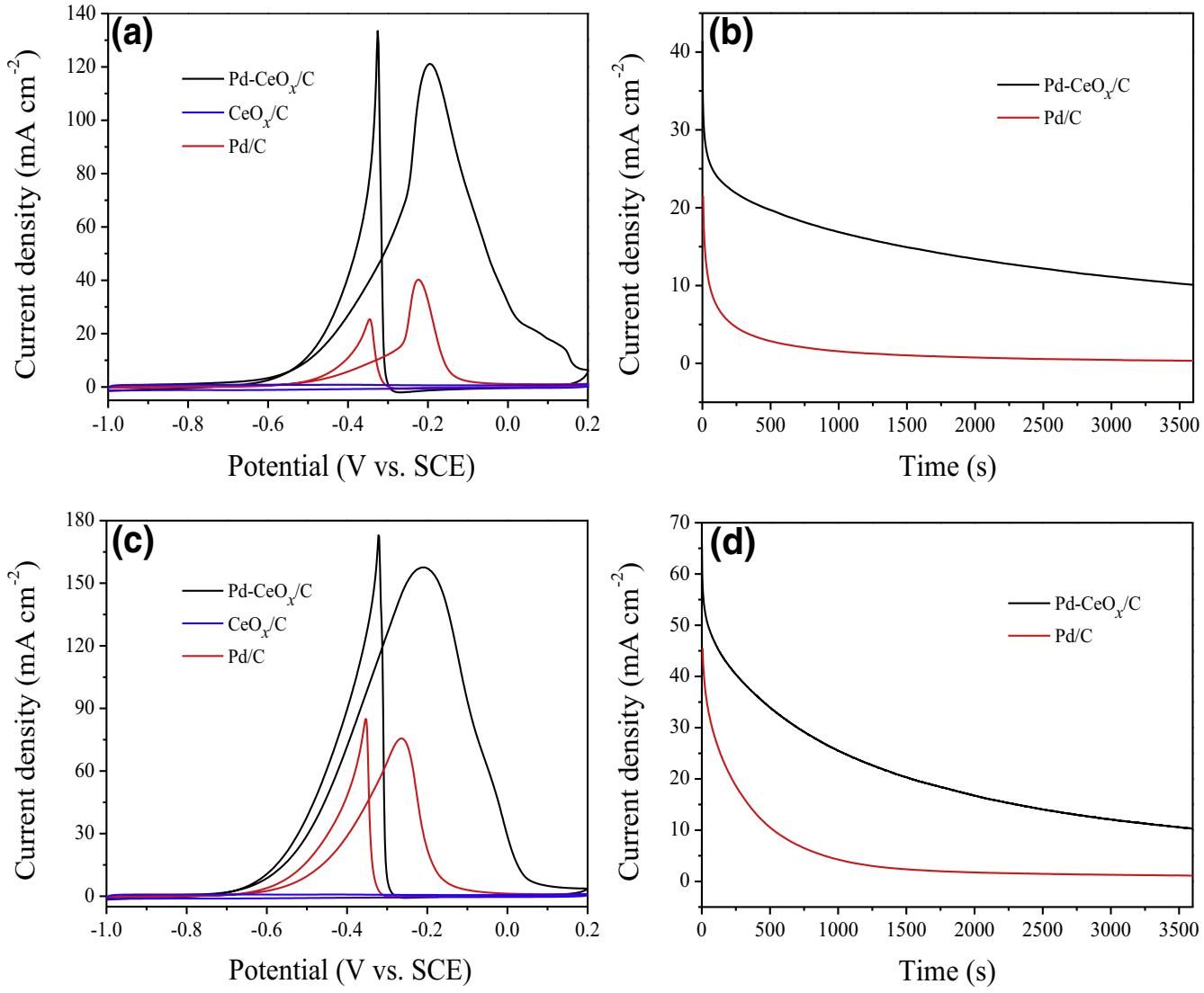

Fig. 6. Cyclic voltammograms of Pd–CeO$_x$/C, CeO$_x$/C and Pd/C catalysts in 1 M KOH/1 M CH_3OH solution (a), and 1 M KOH/1 M C_2H_5OH solution (c) with a sweep rate of 50 mV s^{-1}; chronoamperometry curves of Pd–CeO$_x$/C and Pd/C catalysts in 1 M KOH/1 M CH_3OH solution (b), and 1 M KOH/1 M C_2H_5OH solution (d) at −0.24 V, −0.3 V for 3600 s, respectively.

In order to verify the catalytic performance, alcohols of methanol and ethanol electro-oxidation were studied by cyclic voltammetry and chronoamperometry approaches. The background of cyclic voltammograms in 1 M KOH solution for the interested catalyst was shown in Fig. S4; typical electrochemical behavior of palladium was observed with hydrogen adsorption and desorption and Pd redox. For methanol oxidation, the peak current density was 121.4 mA cm^{-2} and 40 mA cm^{-2} respectively for the Pd–CeO$_x$/C and Pd/C catalyst and it was evident that the hybrid support of CeO$_x$/C had negligible current density (Fig. 6(a)). Judging from the peak current density, the catalytic activity for methanol oxidation on Pd–CeO$_x$/C was three times as high as that of Pd/C catalyst. Moreover, the onset potential for methanol oxidation of the Pd–CeO$_x$/C catalyst was −0.54 V, about 80 mV lower than that of the Pd/C catalyst. According to the above active sites analysis in the Pd–CeO$_x$/C system, if the activity of 58% coming from the Pd active sites, it contributed to ca. 23 mA cm^{-2} (taken Pd/C of 40 mA cm^{-2} as references); and the rest ca. 100 mA cm^{-2} should come from the active sites at Pd–CeO$_x$ nano-interface and the normalized current density to 42% of active sites in the system was around 238 mA cm^{-2} (divided by 42% for consistence) about seven times higher than that of 40 mA cm^{-2} for Pd/C catalyst. Thus, the significance of nanostructured interface is obvious and fabrication such kind of active sites as many as possible should be considered during the materials fabrication. If we do not distinguish the different active sites but directly compare the specific activity by normalizing to the electroactive surface area, the current density calculated was 0.96 and 1.7 mA cm^{-2}, which indicated that the specific activity was also increased by ca. two times thanks to the nanostructured boundaries, though the active sites from nanointerface contributed only ca. 42% based on the CO stripping results. The catalytic stability for methanol oxidation was compared in Fig. 6(b), and it was very clear that Pd–CeO$_x$/C exhibited much better stable trend than that of the Pd/C catalyst. Specifically, the final current density was 10.2 mA cm^{-2} and 0.4 mA cm^{-2} respectively for the Pd–CeO$_x$/C and Pd/C catalyst after 3600 s. The normalized stability was calculated by referencing to the initial current density, the value was 22% for the Pd–CeO$_x$/C, about 4.6 times higher than that of the Pd/C catalyst.

Similar case was also observed when the catalysts were used for ethanol oxidation (Fig. 6c). The peak current density in the forward direction was 158 mA cm^{-2}, about 2.1 times higher than that of Pd/C catalyst (75 mA cm^{-2}); similar case with negligible current density was observed for CeO$_x$/C in ethanol oxidation. Furthermore,

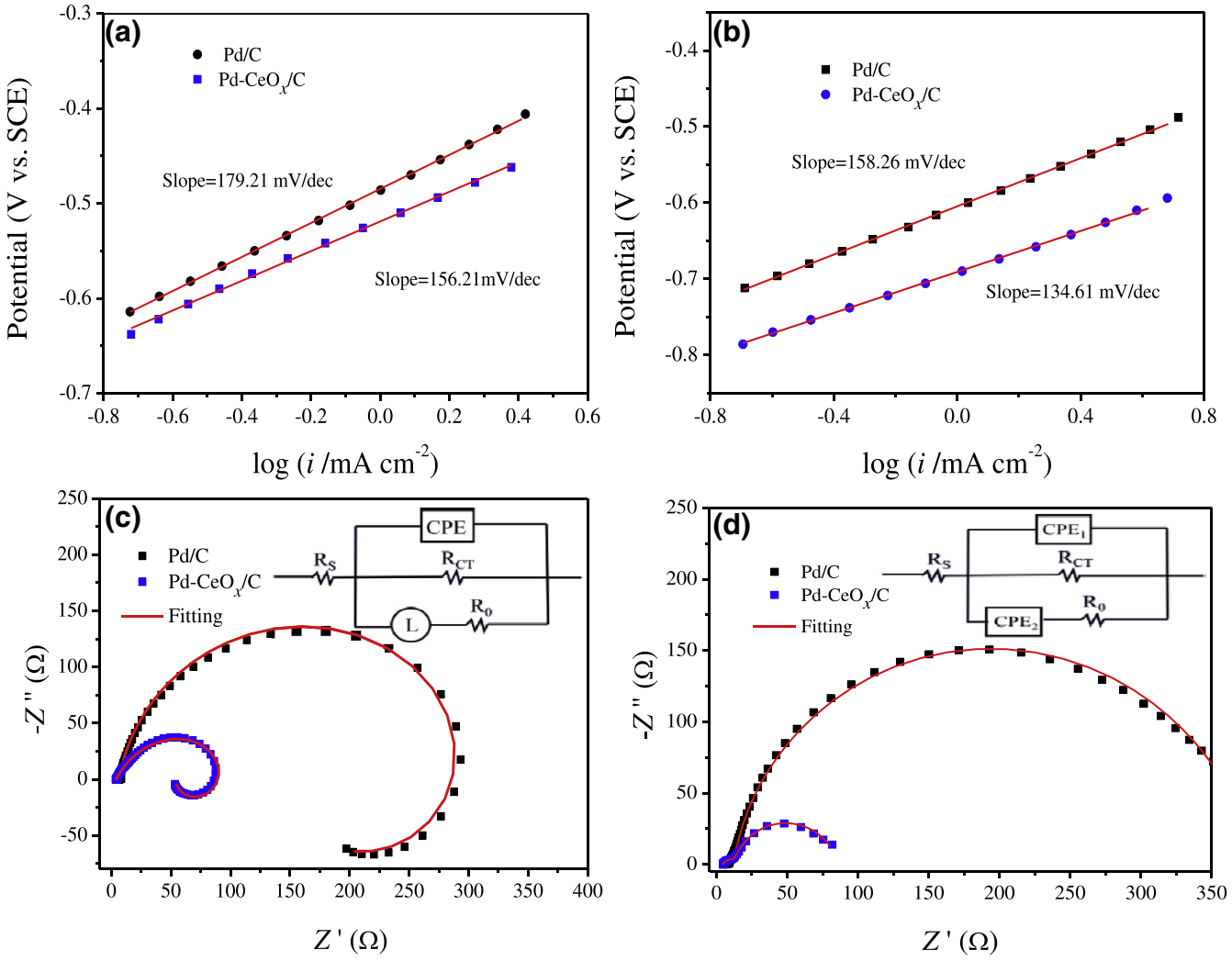

Fig. 7. Tafel plots of Pd–CeO_x/C and Pd/C catalysts in 1 M KOH/1 M CH_3OH solution (a), and 1 M KOH/1 M C_2H_5OH solution (b); Nyquist plots of Pd/C and Pd–CeO_x/C catalysts in 1 M KOH/1 M CH_3OH solution at −0.3 V (insert is the electrical equivalent circuit) (c), and Nyquist plots of Pd/C and Pd–CeO_x/C catalysts in 1 M KOH/1 M C_2H_5OH solution at −0.3 V (insert is the electrical equivalent circuit) (d).

the current density of Pd–CeO_x/C catalyst was also larger than the Pd based catalyst in the literature such as the peak current of 85 mA cm^{-2} [39], 69.3 mA cm^{-2} [40], 68.71 mA cm^{-2} [41] and 64.2 mA cm^{-2} [42]. If we take the same approaches to analyze performance origin, the catalytic efficiency of newly formed interface active sites was ca. 3.6 times higher than that of Pd/C catalyst; it was lower than that of seven-fold for methanol oxidation due to the more complicated and difficult process for ethanol oxidation [43]. The specific activity normalized to the electroactive surface area was 2.21 and 1.8 mA cm^{-2} respectively indicating the more active of the co-action of Pd–CeO_x in the catalyst system. Moreover, a much negative shift of the onset potential for ethanol oxidation was also observed on Pd–CeO_x/C catalyst compared with Pd/C sample. The highly improved catalytic stability for ethanol oxidation was also observed on Pd–CeO_x/C catalyst when compared with Pd/C catalyst (Fig. 6d). After 3600 s, the current density of Pd–CeO_x/C was 10.3 mA cm^{-2}, about 7.9 times higher than that of Pd/C catalyst. Here, taken all together, it was confirmed that the catalytic activity and stability of Pd/C catalyst for alcohols electrooxidation was greatly improved by adding CeO_x in the catalyst system.

As we know that the sluggish kinetics of alcohols oxidation is a serious point that hinder the performance improvement, the kinetics and mechanism revealed by electrochemical measurements was further studied. The Tafel slope of Pd–CeO_x/C and Pd/C catalyst for methanol and ethanol oxidation was shown in Fig. 7(a) and (b), respectively. It was observed that Tafel slope in both methanol and ethanol oxidation for Pd–CeO_x/C was smaller than that of Pd/C catalyst indicating an improved kinetics for the alcohols oxidation. It should be noted that the difference of the slope value for these two catalysts was small, the improved kinetics probably coming from the change of the adsorption amounts of reactive alcohol molecules as the adsorption of oxygen containing species became easier on the cerium oxide.

Impedance was employed to probe the reaction kinetics during the electrocatalysis process and the corresponding Nyquist plots at different potentials were shown in the Fig. S5 with a typical behavior for alcohols oxidation. As the potential increased to −0.6 V, the shape of the Nyquist plots transferred from a straight line to an arc which was consistent with the cyclic voltammetry behavior and it was indicative of the increased kinetics for alcohols oxidation. From −0.5 V to −0.3 V, the shape of the Nyquist plots changed to a semicircle which was related to charge transfer resistance. The minimal diameter was observed at −0.3 V that is an indication of the smallest charge transfer resistance and the highest kinetics for alcohols oxidation. With the further increase of the potential (−0.2 V to −0.1 V), due to the passivation and poisoning of Pd active sites, the increased resistance can be observed. The minimal charge transfer resistance was observed at −0.3 V for

both methanol and ethanol oxidation with a bit little hysteresis as observed in the CV curves. The Nyquist plots for the impedance data collected at −0.3 V on these two electrodes were shown in the Fig. 7(c) and (d) respectively for methanol and ethanol oxidation. The charge transfer resistance was correlated to the semicircle or arc diameter; namely the large the diameter, the larger the charge transfer resistance. The electrochemical impedance data were fitted by an equivalent circuit (inset in Fig. 7(c) and (d)). The electrochemical elements in the circuit have the universal meaning in which R_S represents the uncompensated solution resistance, R_{CT} corresponds to the charge-transfer resistance arising from alcohols oxidation, R_0 is probably related to the contact resistance between the catalyst material and the glassy carbon electrode. Constant phase element (CPE) composition for double-layer capacitance was necessary in the equivalent circuit; and one more CPE was necessary for a better fitting due to the more complicated process in ethanol oxidation; and an inductors L was needed in the case for methanol oxidation that is not normally involved in electrochemical processes usually caused by an external circuit inductance. The data obtained from the electrical equivalent circuit was compared in Tables S1 and S2; the R_S value for all the catalyst materials was round 5 Ω cm^{-2}, and it was evident that in both conditions Pd–CeO_x/C catalyst showed much smaller diameter than that of the Pd/C catalyst. So Pd–CeO_x/C catalyst had much faster charge transfer rate during the alcohols oxidation, and hence greatly improved catalytic activity was observed.

From the above physical characterization and electrochemical measurements, we can see that the introduction of cerium oxide into Pd/C system greatly increased the catalytic activity and stability for alcohols oxidation. Actually the catalytic performance origin of Pd–cerium oxide system was quite complex, it refers to the several factors, e.g., catalyst dispersion, particle size, electronic effect, effect of oxygen vacancies and state of cerium and discussions in details can be seen in some previous reports [29,30]. Anyway, the origin of the performance improvement is absolutely attributed to the co-action of Pd and CeO_x in the catalyst system as each single component cannot guarantee the high catalyst performances. According to our current work, the co-action of Pd and cerium oxide arising from the intimate connection could form the active interface that can be efficient for alcohols oxidation according to the bi-functional mechanism and electronic effect [29]. The performance attribution from different active sites to the catalytic ability for the alcohols oxidation was first analyzed, and the catalytic efficiency was greatly improved on the co-action of Pd and cerium oxide compared with Pd active sites alone. From the morphology and XPS analysis, the nano-interface connection of Pd, cerium oxide and carbon was well supported and the active sites can be probed through the electrochemical CO stripping voltammetry. When the alcohols oxidation was carried on this kind of catalyst, the boundary active sites arising from different components synergy was quite active and robust in the catalysis process.

4. Conclusions

Nanostructured palladium and palladium–cerium oxide catalysts were comparatively studied to probe the origin of performance improvements in catalysis reaction; two kinds of active sites were formed in the nanostructured Pd–cerium oxide system and it was found that the active sites from nanostructured interface connection of Pd and cerium oxide were much more active for alcohols oxidation. The active sites from nanostructured interface were consistently supported by HRTEM and electrochemical CO stripping techniques. Electrochemical measurements from CV, CA and impedance demonstrated the active sites from nanostructured interface were also in favor of the catalytic activity, stability and anti-poisoning ability. In light of the substantial role of nanostructured interface in the hybrid catalyst, more attention should be carefully paid to the active interface design and fabrication in the advanced hybrid catalyst system.

Conflict of interest

There are no conflicts of interest to declare.

Acknowledgments

The work is supported by the National Natural Science Foundation of China (21603041); the Priority Academic Program Development of Jiangsu Higher Education Institution.

Supplementary materials

Supplementary material associated with this article can be found, in the online version, at doi:10.1016/j.jechem.2017.12.011.

References

[1] A. Rabis, P. Rodriguez, T.J. Schmidt, ACS Catal. 2 (2012) 864–890.
[2] L. Feng, H. Xue, ChemElectroChem 4 (2017) 20–34.
[3] J. Chang, L. Feng, K. Jiang, H. Xue, W.-B. Cai, C. Liu, W. Xing, J. Mater. Chem. A 4 (2016) 18607–18613.
[4] M. Choun, J. Lee, J. Energy Chem. 25 (2016) 683–690.
[5] R. Kannan, A.R. Kim, H.-K. Lee, D.J. Yoo, J. Nanosci. Nanotechnol. 15 (2015) 5711–5717.
[6] R. Kannan, A.R. Kim, K.S. Nahm, H.-K. Lee, D. Jin Yoo, Chem. Commun. 50 (2014) 14623–14626.
[7] S. Wang, J. Chang, H. Xue, W. Xing, L. Feng, ChemElectroChem 4 (2017) 1243–1249.
[8] F. Zhang, D. Zhou, M. Zhou, J. Energy Chem. 25 (2016) 71–76.
[9] J. Chang, L. Feng, C. Liu, W. Xing, X. Hu, Energy Environ. Sci. 7 (2014) 1628–1632.
[10] J. Chang, L. Feng, C. Liu, W. Xing, ChemSusChem 8 (2015) 3340–3347.
[11] K. Wang, B. Wang, J. Chang, L. Feng, W. Xing, Electrochim. Acta 150 (2014) 329–336.
[12] R. Kannan, A.R. Kim, K.S. Nahm, D.J. Yoo, Int. J. Hydrogen Energy 41 (2016) 6787–6797.
[13] R. Kannan, A.R. Kim, D.J. Yoo, J. Appl. Electrochem. 44 (2014) 893–902.
[14] M. Xiao, L. Feng, J. Zhu, C. Liu, W. Xing, Nanoscale 7 (2015) 9467–9471.
[15] Q. Wang, H. Tao, Z. Li, C. Chen, S. Liu, L. Han, X. Lu, J. Energy Chem. 25 (2016) 811–816.
[16] N. Cheng, M. Norouzi Banis, J. Liu, A. Riese, S. Mu, R. Li, T.-K. Sham, X. Sun, Energy Environ. Sci. 8 (2015) 1450–1455.
[17] L. Feng, J. Chang, K. Jiang, H. Xue, C. Liu, W.-B. Cai, W. Xing, J. Zhang, Nano Energy 30 (2016) 355–361.
[18] N. Kakati, J. Maiti, S.H. Lee, S.H. Jee, B. Viswanathan, Y.S. Yoon, Chem. Rev. 114 (2014) 12397–12429.
[19] J. Chang, L. Feng, C. Liu, W. Xing, X. Hu, Angew. Chem. Int. Ed. 53 (2014) 122–126.
[20] F. Wang, H. Xue, Z. Tian, W. Xing, L. Feng, J. Power Sour., 375 (2018) 37–42.
[21] W. Huang, H. Wang, J. Zhou, J. Wang, P.N. Duchesne, D. Muir, P. Zhang, N. Han, F. Zhao, M. Zeng, J. Zhong, C. Jin, Y. Li, S.-T. Lee, H. Dai, Nat. Commun. 6 (2015) 10035.
[22] H. Ali, F.K. Kanodarwala, I. Majeed, J.A. Stride, M.A. Nadeem, ACS Appl. Mater. Interfaces 8 (2016) 32581–32590.
[23] Y. Ren, S. Zhang, H. Fang, X. Wei, P. Yang, J. Energy Chem. 23 (2014) 801–808.
[24] H. Huang, Q. Chen, M. He, X. Sun, X. Wang, J. Power Sour. 239 (2013) 189–195.
[25] F. Hu, F. Ding, S. Song, P.K. Shen, J. Power Sour. 163 (2006) 415–419.
[26] C. Roth, A.J. Papworth, I. Hussain, R.J. Nichols, D.J. Schiffrin, J. Electroanal. Chem. 581 (2005) 79–85.
[27] Y.L. Qin, Y.C. Liu, F. Liang, L.M. Wang, ChemSusChem 8 (2015) 260–263.
[28] V. Bambagioni, C. Bianchini, Y. Chen, J. Filippi, P. Fornasiero, M. Innocenti, A. Lavacchi, A. Marchionni, W. Oberhauser, F. Vizza, ChemSusChem 5 (2012) 1266–1273.
[29] E.A. Monyoncho, S. Ntais, N. Brazeau, J.-J. Wu, C.-L. Sun, E.A. Baranova, ChemElectroChem 3 (2016) 218–227.
[30] W. Yuan, J. Zhang, P.K. Shen, C.M. Li, S.P. Jiang, Electrochim. Acta 190 (2016) 817–828.
[31] S.-H. Ye, J.-X. Feng, G.-R. Li, ACS Catal. 6 (2016) 7962–7969.
[32] D.R. Ou, T. Mori, H. Togasaki, M. Takahashi, F. Ye, J. Drennan, Langmuir 27 (2011) 3859–3866.
[33] S. Chowdhury, K.-S. Lin, Mater. Chem. Phys. 133 (2012) 163–169.
[34] Y. Lykhach, T. Staudt, M.P. Lorenz, R. Streber, A. Bayer, H.P. Steinruck, J. Libuda, ChemPhysChem 11 (2010) 1496–1504.
[35] A. Younis, D. Chu, S. Li, J. Phys. D: Appl. Phys. 45 (2012) 355101.
[36] J. El Fallah, L. Hilaire, M. Roméo, F. Le Normand, J. Electron. Spectrosc. Relat. Phenom. 73 (1995) 89–103.

[37] T. Skála, F. Šutara, M. Cabala, M. Škoda, K.C. Prince, V. Matolín, Appl. Surf. Sci. 254 (2008) 6860–6864.
[38] M. Shao, J.H. Odell, S.-I. Choi, Y. Xia, Electrochem. Commun. 31 (2013) 46–48.
[39] N. Li, Y.-X. Zeng, S. Chen, C.-W. Xu, P.-K. Shen, Int. J. Hydrogen Energy 39 (2014) 16015–16019.
[40] C. Mahendiran, T. Maiyalagan, K. Scott, A. Gedanken, Mater. Chem. Phys. 128 (2011) 341–347.
[41] H. Mao, L. Wang, P. Zhu, Q. Xu, Q. Li, Int. J. Hydrogen Energy 39 (2014) 17583–17588.
[42] H. Rostami, A.A. Rostami, A. Omrani, Int. J. Hydrogen Energy 40 (2015) 10596–10604.
[43] C. Xu, L. Cheng, P. Shen, Y. Liu, Electrochem. Commun. 9 (2007) 997–1001.